JACS
JOURNAL OF THE AMERICAN CHEMICAL SOCIETY
Article
Cite This: J. Am. Chem. Soc. 2018, 140, 10881−10889
pubs.acs.org/JACS

A Semiconducting Conjugated Radical Polymer: Ambipolar Redox Activity and Faraday Effect

Pan Wang,[†,‡] Sibo Lin,[†] Zhou Lin,[†] Martin D. Peeks,[†,‡] Troy Van Voorhis,[†] and Timothy M. Swager*[,†,‡]

[†]Department of Chemistry, Massachusetts Institute of Technology, Cambridge, Massachusetts 02139, United States
[‡]Institute for Soldier Nanotechnologies, Massachusetts Institute of Technology, Cambridge, Massachusetts 02139, United States

Supporting Information

ABSTRACT: Investigations of magnetism in electronically coupled polyradicals have largely focused on applications in photonic and magnetic devices, wherein radical polymers were found to possess molecularly tunable and cooperative magnetic properties. Radical polymers with nonconjugated insulating backbones have been intensively investigated previously; however the integration of radical species into conducting polymer backbones is at an early stage. We report herein 1,3-bisdiphenylene-2-phenylallyl (BDPA)-based conjugated radical polymers that display ambipolar redox activities and conductivities. Moreover, these radical polymers were demonstrated to be promising magneto-optic (MO) materials with Faraday rotations wherein the sign is modulated by the radical character and display absolute Verdet constants up to $(2.80 \pm 0.84) \times 10^4$ deg T^{-1} m^{-1} at 532 nm. These values rival the performance of the present-day commercial inorganic MO materials (e.g., terbium gallium garnet, $V = -1.0 \times 10^4$ deg T^{-1} m^{-1} at 532 nm). The structure property studies detailed herein reveal the promise of multifunctional conjugated radical polymers as responsive MO materials.

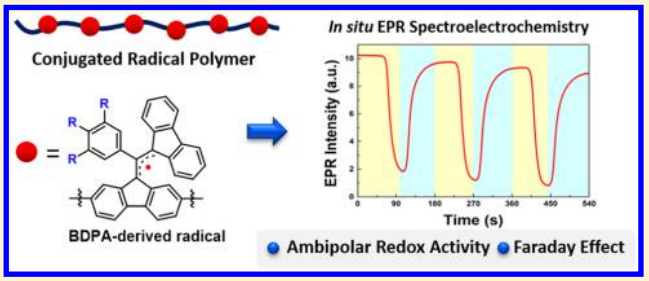

1. INTRODUCTION

Polymer magnetism[1] is both promising and challenging. Polyradicals have been investigated as molecular magnets, elements in organic electronics and photonic/magnetic devices,[2] and redox-active elements for battery technologies.[3] Noteworthy investigations of molecular magnetism in radical polymers date back to 1980s, wherein cooperative magnetic phenomena arising from spin conduction through chemical bonds and ferromagnetism in organic materials were proposed.[4] Faraday rotation, the rotation of the plane-polarized light due to magnetic-field-induced circular birefringence, is an interesting and useful magnetic phenomenon displayed strongly by inorganic ferromagnetic materials.[5] Inorganic magneto-optic (MO) materials are widely used in magnetic photonics[6] and magnetic field sensors;[2d,7] however the application of organic MO materials has not progressed as a result of their poor performance at telecommunication wavelengths (e.g., 1550 nm).[8] However, the growing interest in tunable and flexible electronic devices with properties that can be tailored at the molecular level continues to inspire the development of organic materials to replace rigid inorganics.[9] This demand has stimulated recent MO studies on closed-shell π-conjugated polymers,[10] and the effect of radicals on Faraday rotation has been studied by introducing small molecular radicals blended with a polymer;[11] nevertheless the dearth of stable open-shell semiconducting radical polymers has limited their exploration. Understanding the nature of spin coupling and electronic delocalization in radical polymers is beneficial to the development of organic MO materials for photonic and magnetic applications.

Radical polymers with half-filled states at their Fermi levels are expected to show redox activity, optoelectronic activity, and magnetic properties.[3a−c] The majority of open-shell polymers have pendant stable modular radical groups attached to a nonconjugated insulating backbone (Figure 1a).[3b,12] Although these materials have shown appropriate utility, the localized nature of the spin states and the lack of coupling to extended and highly polarizable π-electronic states limit their MO properties. In contrast, radicals that are electronically coupled with conjugated backbones[13] have the potential to couple more strongly to magnetic fields and are also natural ambipolar redox-active materials, capable of hole and electron transport. Polyacetylenes have been one of the favored π-conjugated scaffolds upon which to append radicals, and other preferred structures include polydiphenylamine[13c] and polythiophenes (Figure 1a).[13a,b] Pendant radical groups that have been introduced to the conjugated backbones include 2,2,6,6-tetramethylpiperidinyl-1-oxyl (TEMPO), aminyloxyl, phenoxyl, and galvinoxyl radical groups. We have had an interest in 1,3-bisdiphenylene-2-phenylallyl (BDPA) radical,[14] one of the most stable and long-lived carbon-centered radicals,[15] and applications of its derivatives. There have been limited efforts to create materials incorporating this radical, and noteworthy is

Received: June 12, 2018
Published: August 21, 2018

DOI: 10.1021/jacs.8b06193
J. Am. Chem. Soc. 2018, 140, 10881−10889

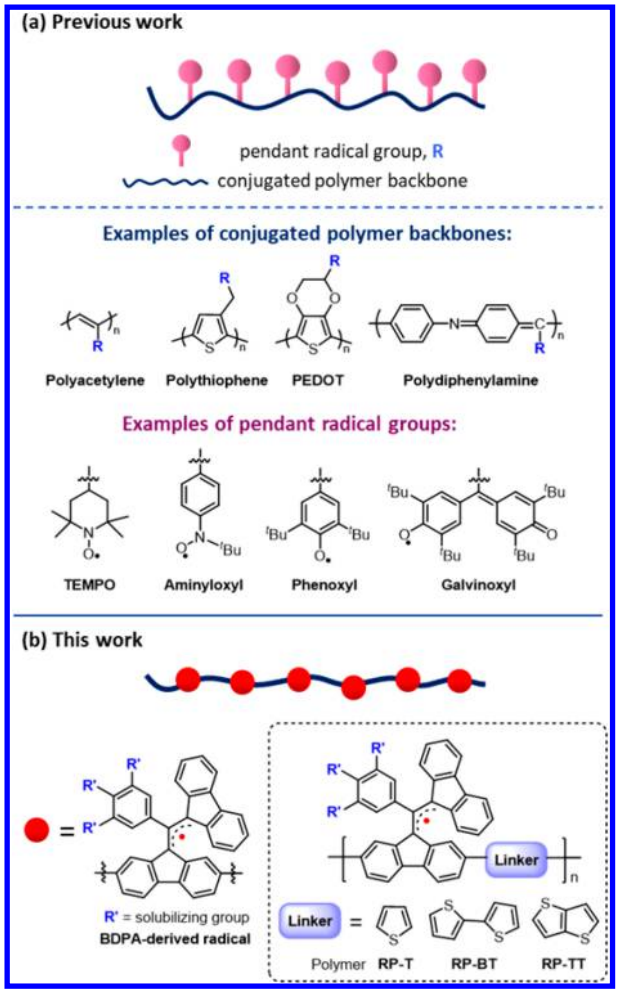

Figure 1. Schematic representation of conjugated radical polymers.

the report of Nishide et al., who prepared polyacetylene with pendant BDPA groups in 1992.[16] The stability and redox activity of this long-lived radical are very attractive for the realization of new generations of materials with electrical conductivity and MO activity.

Herein, we report the synthesis of BDPA-based ambipolar redox-active conjugated radical polymers and the characterization of their properties by *in situ* electron paramagnetic resonance (EPR) and UV−vis spectroelectrochemistry (Figure 1b). Reduction of the radical polymers affords anionic materials, and conversely, they can be oxidized to cationic forms. We have further profiled their conductivity as a function of oxidation state by fabricating microelectrochemical transistors and have demonstrated that the radical polymers are more conductive than their nonradical analogues. The measurement of Faraday rotation allowed us to evaluate the MO activities of the radical polymers and revealed a strong relationship between the radical character and the sign of Faraday rotation. The Faraday effect was characterized by high Verdet constants (V, the quantification of MO activity), which rival the current top widely applied inorganic materials (e.g., terbium gallium garnet (TGG), $V = -1.0 \times 10^4$ deg T^{-1} m^{-1} at 532 nm).[8]

2. MATERIALS DESIGN AND SYNTHESIS

BDPA-derived radicals and their oligomers have utility.[17] In particular, BDPA and its derivatives are robust radicals for microwave-driven dynamic nuclear polarization (DNP) for the enhancement of NMR signals.[18] The materials of interest here are derived from BDPA core structures that are copolymerized with thienyl groups to give the structures shown in Scheme 1. The polymerization makes use of the formally hydrogenated precursors to the BDPA radical as the monomer to avoid possible side reactions of the radicals in the polymerization process. Once synthesized, the polymer was transformed into radical forms via deprotonation and oxidation. Following Kuhn and Neugebauer's synthetic methods,[19] 2,7-dibromo-BDPA-H was synthesized and subjected to Stille-coupling polymerization with 2,5-bis(trimethylstannyl)thiophene. The initial polymer **BDPA-P1** was relatively insoluble in most organic solvents, and the number-average molecular weight (M_n) of the tetrahydrofuran (THF)-soluble portion was estimated to be 14.9 kDa by gel permeation chromatography (GPC) with a narrow polydispersity ($Đ$) of 1.17. To increase the solubility, we sought to install long alkyl chains onto the phenyl ring pendant to the BDPA core structure. However, the established synthetic methods were not compatible with the electron-rich phenyl ring, and Kuhn's pathway to the BDPA molecule failed. Specifically, it appears that these groups prevented a key dibromination reaction (Scheme S3).

To produce an expanded scope of BDPA analogues, we developed a more general synthetic pathway that accommodates electron-rich substrates (Scheme 2). In the new synthetic route, a trialkoxy diethyl(α-chlorobenzyl)phosphonate (**3**) is synthesized as the key precursor. This compound is produced from the corresponding benzyl aldehyde, which is subjected to the Pudovik reaction under the conditions of a catalytic amount of *n*-butyllithium to give diethyl(α-hydroxybenzyl)phosphonate (**2**). Conversion of the hydroxyl to a chlorine produces **3** and results in excellent yield. Compound **3** is then reacted with fluorenone via a Horner−Wadsworth−Emmons reaction to generate compound **4** in 54% yield. Conjugate addition of the deprotonated anion from 2,7-dibromofluorene to **4** affords monomer **5** as two isomers with 82% yield (**5a**/**5b** = 1/5). This synthetic pathway allows for gram-scale synthesis of **5a** and **5b**. Stille coupling polymerization of **5a** and **5b** with different thienyl distannanes provides BDPA-based polymers. The polymerization of **5** (a mixture of isomers **5a** and **5b**) with 2,5-bis(trimethylstannyl)-thiophene gave polymer **P-T** in 96% yield with a high molecular weight of 35 kDa ($Đ$ = 2.70). Using different comonomers, polymers **P-BT** and **P-TT** were synthesized in quantitative yields with molecular weights of 55.3 kDa ($Đ$ = 3.96) and 21.1 kDa ($Đ$ = 2.41), respectively.

Scheme 1. Synthetic Strategy of BDPA-Based Radical Polymers

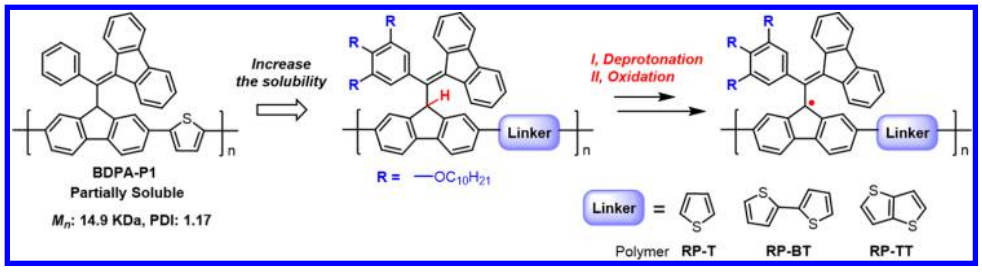

DOI: 10.1021/jacs.8b06193
J. Am. Chem. Soc. 2018, 140, 10881−10889

Scheme 2. Synthetic Pathway of Monomers and Radical Polymers[a]

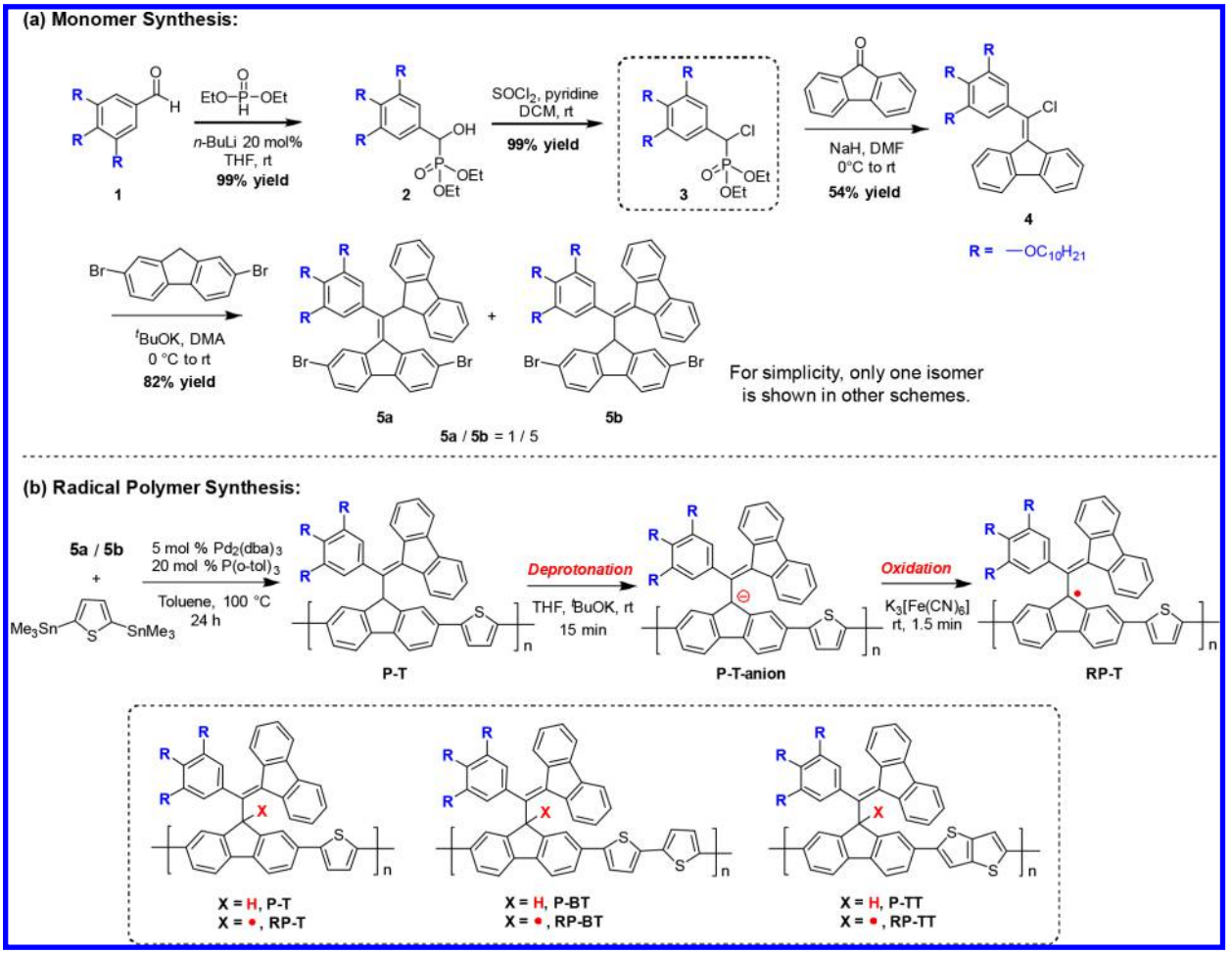

[a]Note that the repeating units of radical polymers are not 100% radical species; incomplete oxidation exists based on the spin concentrations by EPR measurements.

Table 1. Physical Properties of BDPA-Based Radical Polymers

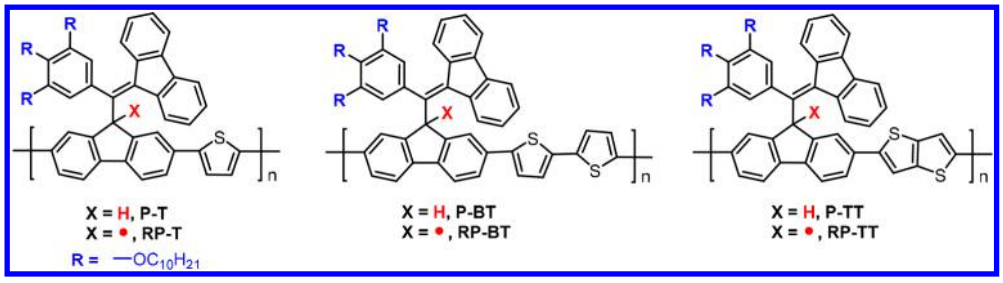

polymer	yield (%)[a]	M_n (kDa)/PDI[b]	T_d (°C)[c]	λ_{max} solution (nm)[d]	spin concentration[e] x mol %
P-T	96	35.0/2.70	406	434	
RP-T		25.7/4.78	434	433, 865	39
P-BT	95	55.3/3.96	410	465	
RP-BT		39.0/4.36	390	453, 864	17
P-TT	99	21.1/2.41	438	448	
RP-TT		18.7/5.40	433	459, 857	26

[a]Yields of hydrogenated polymers are yields of polymerization steps; yields of radical polymers are not shown, as the oxidation reactions are incomplete. [b]Evaluated by gel permeation chromatography (GPC) in THF against a polystyrene calibration at room temperature. [c]Decomposition temperature. [d]In THF solution. [e]Polymers were dissolved in toluene with a concentration of 1.0 mM (TEMPOL was used as an external standard).

The corresponding radical polymers **RP-T**, **RP-BT**, and **RP-TT** were prepared by deprotonation of the proton at the benzylic position of fluorene with excess potassium *tert*-butoxide (4 equiv), followed by oxidation of BDPA anions to radicals using potassium ferricyanide (6 equiv) to ensure a more complete oxidation process. We find that the resulting radical polymers are less soluble with extended oxidation

DOI: 10.1021/jacs.8b06193
J. Am. Chem. Soc. 2018, 140, 10881−10889

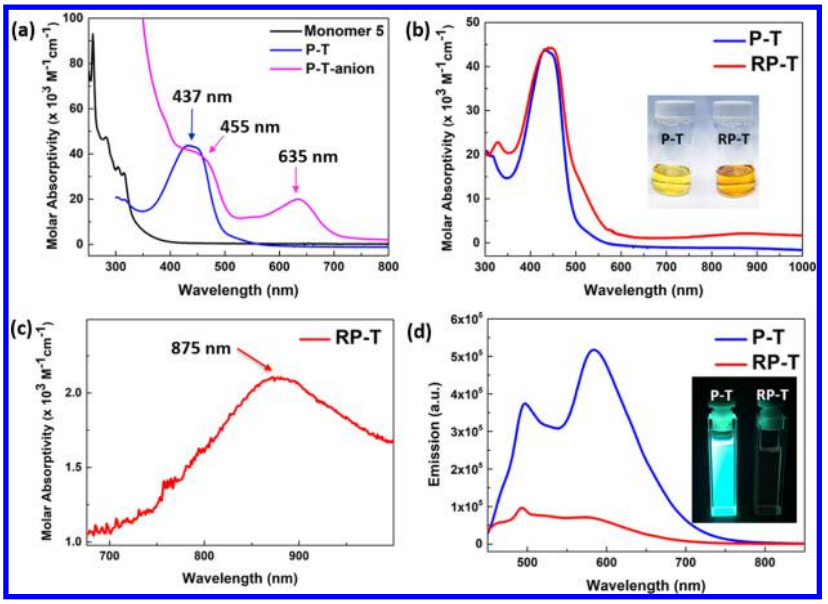

Figure 2. Absorption and emission spectra measured in THF. (a) Absorption spectra of monomer **5**, **P-T**, and **P-T-anion**. (b) Comparison of UV–vis absorption of **P-T** and **RP-T** with concentrations of 0.02 mg/mL. (c) Inset of the absorption spectra of **RP-T**, showing the enlarged spectra between 675 and 1000 nm. (d) Comparison of emission bands of **P-T** and **RP-T**, excitation wavelength: 440 nm.

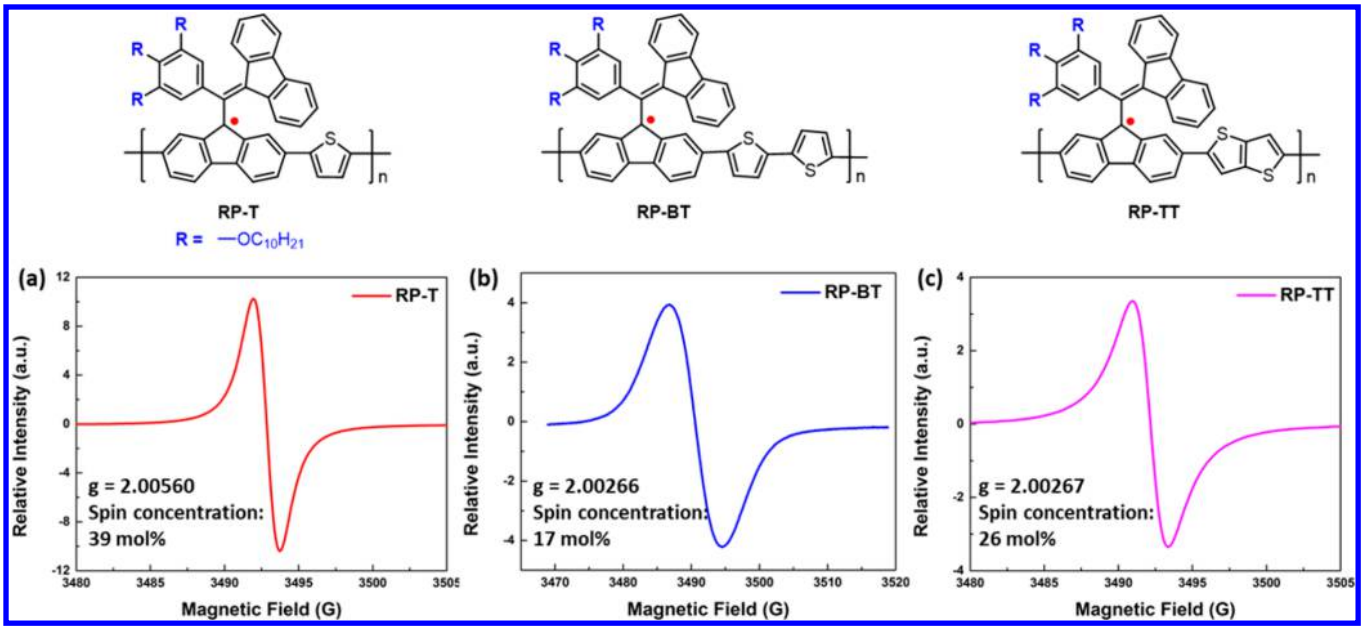

Figure 3. EPR spectra of radical polymers (a) **RP-T**, (b) **RP-BT**, and (c) **RP-TT** in toluene at 298 K. Polymers were dissolved in toluene with a concentration of 1.0 mM (TEMPOL was used as an external standard).

time and become completely insoluble after 30 min. This effect is likely the result of higher intermolecular interactions between the π-systems and/or cross-linking of the polymers. After optimization, we have adopted an oxidative time of 1.5 min, which probably gives incomplete oxidation, but maintains the necessary solubility for our studies. This issue is likely the origin of different spin concentrations in the radical polymers (*vide infra*). Nevertheless, although the obtained radical polymers as prepared exhibit good solubility in organic solvents, vacuum drying at room temperature for an extended time (e.g., 3 days) still results in problematic limited solubility.

The physical properties and characterization data of **RP-T**, **RP-BT**, and **RP-TT** are summarized in Table 1. The obtained red-colored radical polymers only showed broad ^{1}H NMR signals of the alkyl chains on the phenyl ring, but no proton signals in the aromatic region even at a concentration of 25 mM in chloroform-*d*. Hence the radical concentration is sufficient to broaden most of the proton signals associated with the π-system to the levels where they are not detectable. Different absorption and emission behaviors were observed among the monomer, the as-synthesized nonradical polymers, the polymer anions, and the polymer radicals. The spectra are illustrated in Figure 2, and the differences are readily visualized.

Monomer **5** is colorless with an absorption band around 300 nm in THF, whereas the solution of **P-T** in THF is red-colored with an absorption band at 437 nm. The addition of an excess amount of potassium *tert*-butoxide immediately changes the red solution of **P-T** to deep blue. The resulting anionic polymer, **P-T-anion**, has an absorption band at 455 nm and a new absorption band at 635 nm (Figure 2a). Oxidation by potassium ferricyanide transforms the deep blue solution to dark red, indicating the formation of radical species **RP-T**. The absorption of **RP-T** is similar to that of **P-T** in general, but

DOI: 10.1021/jacs.8b06193
J. Am. Chem. Soc. 2018, 140, 10881–10889

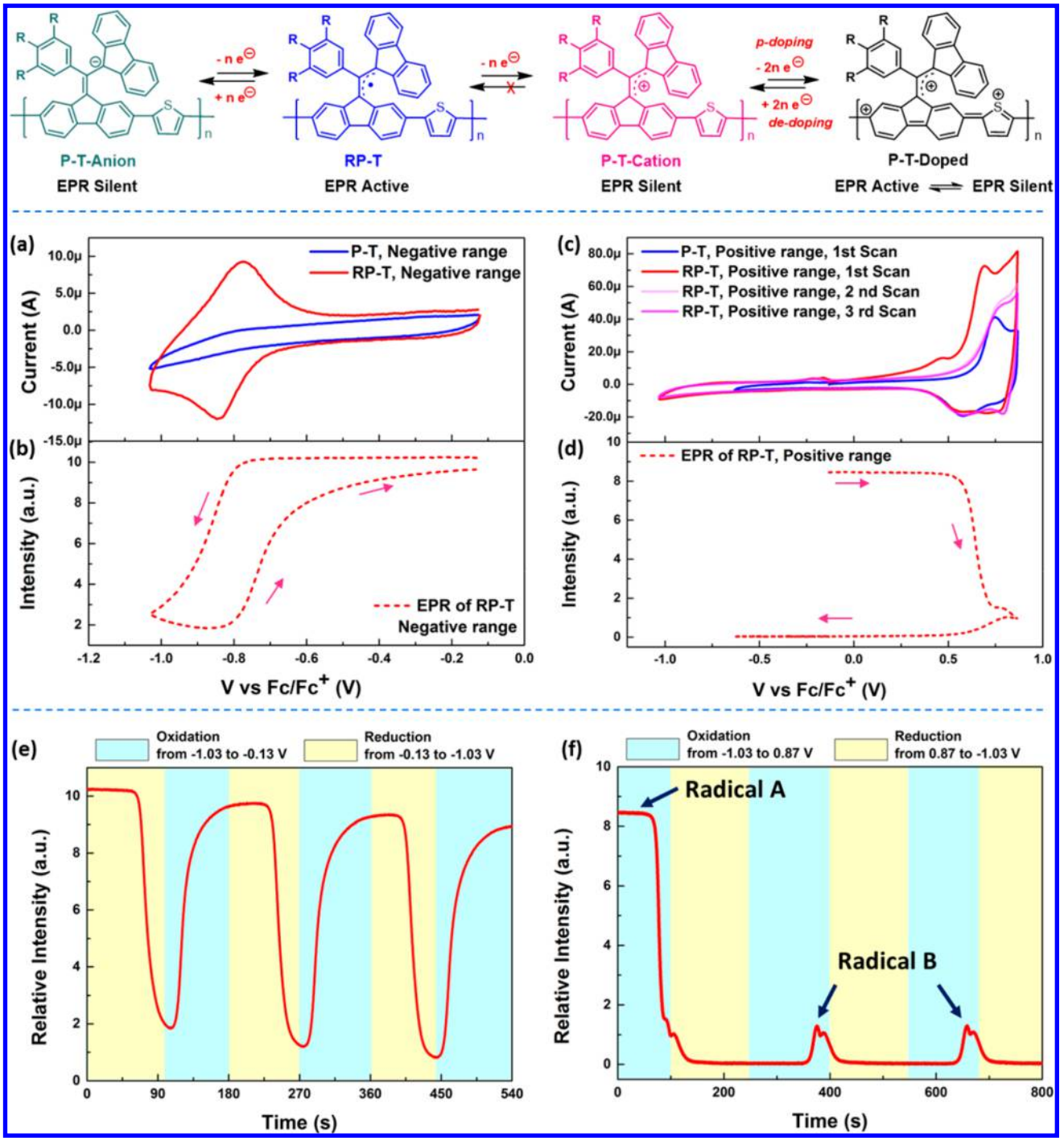

Figure 4. EPR spectroelectrochemistry of **P-T** and **RP-T** coated on Pt wire as the working electrode (0.1 M Bu_4NPF_6 in CH_3CN was used as the electrolyte, Pt wire as the counter electrode, and $Ag/AgNO_3$ as the reference electrode). Scan rate: 10 mV/s. Ferrocene was used as external standard. CV and EPR were taken in a flat cell quartz EPR tube as shown in Figure S11. (a) CVs of negative scan between −1.03 and −0.13 V; (b) EPRs of negative scan between −1.03 and −0.13 V; (c) CVs of positive scan between −1.03 and 0.87 V; (d) EPRs of positive scan between −1.03 and 0.97 V. EPR intensity change in the process of (e) negative scans and (f) positive scans.

contains a weak absorption band between 500 and 550 nm and a new broad absorption band around 875 nm (Figure 2b and c). The latter confirms the formation of BDPA radicals, as the molecular BDPA radical displays a similar molar absorptivity around 859 nm.[19,20] Polymer **P-T** shows two emission bands at 496 and 584 nm, and as expected the emission of **RP-T** is almost entirely quenched (Figure 2d) probably as a result of a singly occupied molecular orbital (SOMO)-facilitated electron transfer.[21] Similar absorption and emission phenomena were also observed in radical polymers **RP-BT** and **RP-TT** (Figures S1 and S2).

The radical polymers and their hydrogenated analogues display similarly high thermal stabilities, as evaluated by thermal gravimetric analysis (TGA) (Figure S3) with decomposition temperatures in the range of 390−438 °C. Furthermore, the polymers appear to be amorphous with no obvious thermal transitions observed in the range from 100 to 350 °C in the differential scanning calorimetry (DSC) analysis. The amorphous nature of the polymers can be attributed to the bulky trialkoxy BDPA groups along the polymer backbone and their different stereoisomers.

DOI: 10.1021/jacs.8b06193
J. Am. Chem. Soc. 2018, 140, 10881−10889

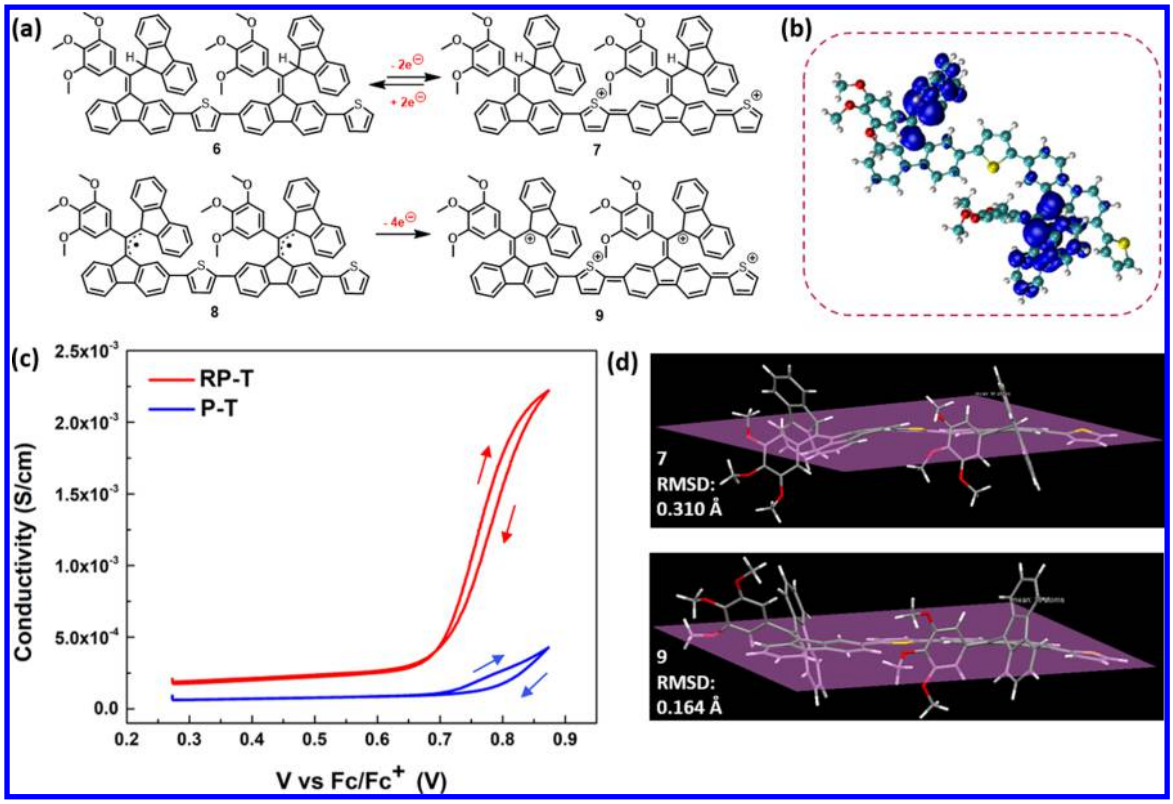

Figure 5. DFT calculations with two repeating units and conductivity mapping with microelectrochemical transistors. (a) Schemes showing structures for dimers **6** and **8** and their model oxidized states **7** and **9**. (b) Spatial distribution of the unpaired electron density on the dimer **8** at its triplet ground state. (c) Conductivity mapping of polymer films using an interdigitated array electrode. Conductivity profiles were recorded with an applied offset potential of 50 mV and a scan rate of 2 mV/s in acetonitrile electrolyte solution. (d) DFT-optimized geometries of the oxidized model dimers **7** and **9**. Methyl groups are used instead of long alkyl chains in the calculations. Root-mean-square deviation (RMSD) is used to measure the average distance between the non-H backbone atoms and the calculated plane using planar regressions.

All polymers show a reversible UV−vis spectroelectrochemical behavior as a function of the applied potential. To prepare for the spectroelectrochemical study, each polymer was spin-coated on an indium tin oxide (ITO)-coated glass, which serves as the working electrode in a three-electrode cell. The UV−vis spectra were measured as a function of the applied potential (Figure S5). In the case of the radical polymer **RP-T**, spectroelectrochemical measurements were taken from 0 to −0.9 V vs Ag/Ag^+ in acetonitrile, and the polymer film undergoes a color change from bright red to dark blue with reduction. As shown in Figure S5a, a decrease in the high-energy absorption band around 430 nm was observed, as the radicals are transformed into anions. An increase of a sharp absorption peak at 628 nm is related to anions, which is consistent with the spectrum of the **P-T-anion** shown in Figure 2a. A small shoulder peak was also observed at 350 nm. Oxidation from 0 to 1 V results in a decrease of the high-energy absorption band around 430 nm and the emergence of a low-energy band around 600 nm (Figure S5b).

3. SOLUTION EPR SPECTRA

The spin densities of **RP-T**, **RP-BT**, and **RP-TT** were quantitatively probed by solution EPR measurements with TEMPOL as an external standard.[22] The radical polymers were dissolved in toluene with a concentration of 1.0 mM (repeating unit), and EPR measurements were conducted at 298 K.

As can be seen from Figure 3, compared to molecular BDPA radical, which shows EPR spectra with hyperfine structure, the three radical polymers exhibit featureless broad EPR spectra. **RP-T** shows a single EPR signal with a *g*-value of 2.005 60 and a narrow peak-to-peak separation of 1.8 G (Figure 3a), and the spin concentration is 39 mol %.[16] **RP-BT** shows an EPR signal with a *g*-value of 2.002 66 and a lower spin concentration of 17 mol %, along with a broader peak-to-peak separation of 7.6 G, whereas **RP-TT** presents an EPR signal with $g = 2.002\,67$ and a spin concentration of 26 mol % with a peak-to-peak separation of 2.4 G. The higher spin concentration in **RP-T** is perhaps the reason for the narrowing of the line width in the EPR signal. The lower spin concentrations of **RP-BT** and **RP-TT** are attributed to the incomplete oxidations mentioned above. BDPA radicals are remarkably stable to oxygen in the solid state, but are less stable to oxygen in solution.[20a] Fortunately, our radical polymers are relatively persistent at room temperature in solution. When protected from light in a capped EPR tube, the EPR signal of **RP-T** in degassed toluene solution exhibits only a 13% decrease in EPR intensity at room temperature after 24 h, probably because of the leak of oxygen (Figure S4a), and the normalized EPR spectra indicate no other radical species is generated (Figure S4b).

4. *IN SITU* EPR SPECTROELECTROCHEMISTRY

To better understand the electrochemical and spin behaviors of the radical polymers, EPR spectroelectrochemistry was conducted. The characteristic EPR signals of BDPA radical were expected to transform into spinless anions and cations upon reduction and oxidation, respectively. Cyclic voltammetry (CV) of the radical form of monomer **5** in solution demonstrated that two reversible redox waves exist at $E_{1/2} = 0.50$ V and $E_{1/2} = -0.78$ V (vs Fc/Fc^+), which is similar to the unsubstituted BDPA radical (Figure S6).[20a] This similarity suggests the solubilizing alkoxy groups on the

DOI: 10.1021/jacs.8b06193
J. Am. Chem. Soc. 2018, 140, 10881−10889

benzene ring have a minimal effect on the radical's redox thermodynamics.

To prepare for EPR spectroelectrochemistry, polymers were dip-coated on thin Pt wire as the working electrode, another Pt wire was used as the counter electrode, and $Ag/AgNO_3$ was used as the reference electrode. The electrolyte (0.1 M Bu_4NPF_6 in CH_3CN) was transferred into a flat cell quartz EPR tube (Figure S11). **RP-T** has a single EPR signal with a narrow peak-to-peak separation of 1.8 G, which is in agreement with our solution EPR results (Figure 3a) and allows for a real-time measurement of EPR signal intensity while sweeping the potential.

Polymer **P-T** and radical polymer **RP-T** exhibit different CV behaviors and EPR spectra in this experiment. For example, the CV of **RP-T** (Figure 4a) shows one reversible reduction/oxidation wave ($E_{1/2}$ = −0.82 V), concomitant with a reversible decrease and increase in EPR intensity (Figure 4b). This behavior can be assigned to BDPA-centered radical/carbanion redox processes in **RP-T**. These waves are absent in the hydrogenated polymer **P-T** over the same potential range. In Figure 4c and d, potential sweeps of **RP-T** from 0 to 0.87 V vs Fc/Fc^+ and back show two oxidation waves around 0.70 and 0.81 V and a return broad reduction wave around 0.63 V. For the second and third oxidative CV cycles of **RP-T**, quasi-reversible oxidation waves appear that are less intense than in the first cycle. After the first oxidative scan to 0.87 V, no electrochemical events are found in the range of 0 to −1.03 V, suggesting that when the radicals in the polymer are oxidized into spinless carbocations, they are kinetically trapped or decompose. This phenomenon is again confirmed by concomitant EPR measurement (Figure 4d), wherein the EPR intensity decays rapidly during the first oxidative sweep and stays at the same level throughout the reductive sweep. After the first oxidative scan, **RP-T** shows a new redox-active feature and a smaller spin density, which based on conductivity data (*vide infra*) are associated with the formation of polarons and bipolarons in the conjugated polymer backbone. EPR spectra of radical **A** and radical **B**, illustrated in Figure 4f, show different line shapes and *g*-values, confirming that they are two different radical species (Figure S7). In the meanwhile, no EPR intensity change is observed in the range of 0 to −1.03 V with hydrogenated polymer **P-T** (Figure S8c), but the formation of polarons is implied by EPR intensity changes in the range of 0 to 0.87 V (Figure S8d).

From the data obtained, we can envision that three different electrochemical processes occur in the radical polymers, as illustrated in Figure 4. In Figure 4e, the reduction and reoxidation of radicals are completely reversible when sweeping the potential in the negative range. EPR-active **RP-T** is transformed to the EPR-silent **P-T-Anion** with reduction. As shown in Figure 4f, sweeping to positive potentials oxidizes the radicals and the **P-T-Cation** becomes irreversibly EPR silent. Further oxidation at higher potentials removes more electrons from the polymer, and any polarons are transformed to bipolarons. This form, **P-T-Doped**, becomes EPR silent again. The doping and dedoping process in the polymer backbone is reversible. Similar observations were also found in radical polymers **RP-BT** and **RP-TT** (Figures S9 and S10).

5. CONDUCTIVITY MAPPING WITH MICROELECTROCHEMICAL TRANSISTORS AND ELECTRONIC STRUCTURE THEORY

We studied the electrical conductivity by *in situ* conductivity measurements on microelectrochemical transistors with Pt interdigitated electrodes (Figure S12). The microelectrochemical transistor[23] is a simple and robust method to examine the conductivity of polymers as a function of electrochemical potential.[24] We tested the performance of both radical polymers and their hydrogenated analogues. As can be seen from Figure 5c, the two polymers display their highest conductivity when at the highest applied potentials. The highest conductivity of p-doped **RP-T** is 2.22 mS/cm, which is considerably higher than 0.42 mS/cm of p-doped **P-T**. At the potential of maximum conductivity, the BDPA-based radicals in **RP-T** have been oxidized into carbocations, which may boost conductivity by increasing the number of charge carriers. Higher conductivities were also observed with **RP-BT** of 2.14 mS/cm and **RP-TT** of 1.68 mS/cm, when compared to the conductivities of their parent hydrogenated polymers **P-BT** and **P-TT**, which possess conductivities of 1.73 and 0.96 mS/cm respectively (Figure S13).

Considering that **P-T** and **RP-T** display the largest difference in electronic conductivity, model compounds containing two repeating units for **P-T** (**6**) and **RP-T** (**8**) and their oxidized forms (**7** and **9**) were studied computationally using density functional theory (DFT) as shown in Figure 5a. As a result of the large size of the BDPA moieties, it is not surprising that the atoms included in the conjugated backbone are distorted from idealized coplanarity, as was reported,[17b] and revealed by DFT geometry optimizations (Figure S14). As a quantitative metric for coplanarity, the root-mean-square deviation (RMSD) (Table S1) of the non-H backbone atoms from the calculated plane was evaluated using planar regressions and resulted in RMSD = 0.579 Å for **6** and 0.451 Å for **8**. Upon formal oxidation from **6** to **7**, the oxidized form **7** enforces a level of nonplanarity (RMSD = 0.310 Å). However, formal oxidation from **8** to **9** results in significantly greater coplanarity and a smaller RMSD of **9** (0.164 Å) (Figure 5d). Therefore, a similar coplanar effect in the corresponding polymers is expected to lead to greater intrachain conductivity and interchain packing in oxidized radical polymers compared to their hydrogenated forms.

The spin configuration and density of **8** were also characterized using the restricted open-shell DFT calculations (Figure 5b). We observed a triplet ground state that is 1.8623 eV lower than the singlet excited state, indicating the EPR-active diradical configurations. As described by the spin density distribution, the negligible spatial overlap between two radical sites further stabilizes the diradical structure of **8**. Upon oxidation or reduction of **8**, the unpaired electrons can be either paired by newly added electrons or removed from the system, bringing EPR silence back to the system. Moreover, the DFT-based simulations of spectroelectrochemistry of the dimer models are included in Figure S15.

6. MAGNETO-OPTIC PROPERTIES: FARADAY ROTATION MEASUREMENT

The present understanding of the MO activity in conjugated polymers is very limited; however, electronic delocalization along the polymer backbone appears to enhance Faraday rotations. Recent MO studies in organic materials have been

DOI: 10.1021/jacs.8b06193
J. Am. Chem. Soc. 2018, 140, 10881−10889

limited to closed-shell π-conjugated polymers, and hence we have performed Faraday rotation measurements on our open-shell polymers. The sensitivity of Faraday effect in MO materials is expressed by Verdet constant (V), which is defined as $\theta = VBL$, where θ is the polarization rotation, B is the applied magnetic field, L is the length of light propagation through the material, and V is wavelength dependent. The MO properties were evaluated using a 532 nm laser diode light source. Glass slides with 170 μm thickness were used as substrates, and the polymers were dissolved in chloroform (15 mg/mL) and spin-coated (1500 rpm) on the surface with

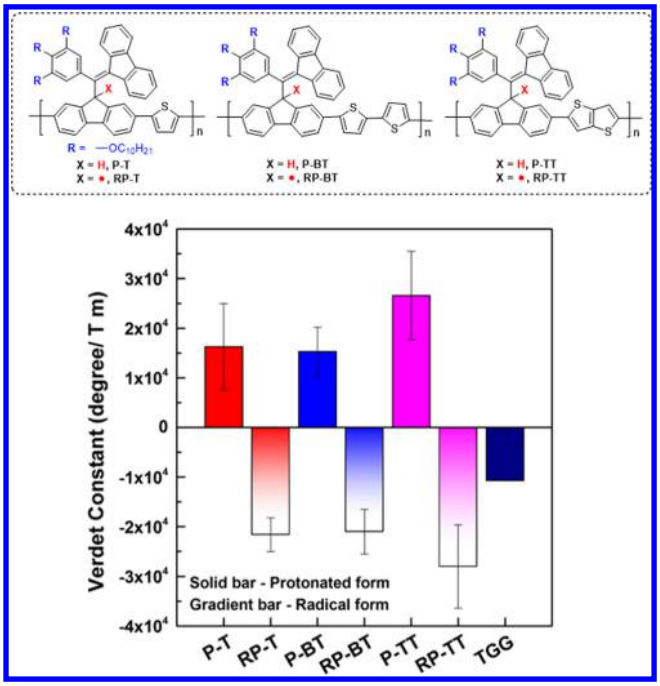

Figure 6. Verdet constants of polymers **P-T**, **P-BT**, and **P-TT** and radical polymers **RP-T**, **RP-BT**, and **RP-TT**. Samples were measured over applied magnetic fields from −0.5 to +0.5 T at 532 nm. Polymers were dissolved in chloroform and spin-coated on 170 μm glass slides. Error bars represent the propagation of errors of background measurements, sample measurements, and film thickness measurements by AFM.

thicknesses between 100 and 150 nm. Our MO spectrometer has been constructed as a hybrid of previously established designs[10a,b] and provided $V = -(1.07 \pm 0.0037) \times 10^4$ deg T^{-1} m^{-1} for the inorganic MO reference material TGG, consistent with the literature reported values.[8]

As shown in Figure 6, polymers **P-T**, **P-BT**, and **P-TT** all possess positive Verdet constants ranging from $(1.53 \pm 0.49) \times 10^4$ to $(2.66 \pm 0.89) \times 10^4$ deg T^{-1} m^{-1}. However, attempts to fabricate thin-film samples from anionic forms of the polymers failed, as the anionic species were quickly quenched by the moisture/oxygen in the air during spin-coating, giving the same level of Verdet constants as their hydrogenated forms. The radical polymers **RP-T**, **RP-BT**, and **RP-TT** were found to give negative Verdet constants ranging from $-(2.10 \pm 0.45) \times 10^4$ to $-(2.80 \pm 0.84) \times 10^4$ deg T^{-1} m^{-1}. The different signs of Verdet constants reflect the different rotation directions of the polarization when the light travels through the materials. We have previously discovered that there is a strong relationship between polymer helical structure and the sign of Faraday rotation.[25] We find here that the direction of Faraday rotation can also be controlled by the spin state (BDPA$^{\bullet}$/BDPA-H) of the polymer. The hydrogenated parent diamagnetic polymers display Faraday rotations via mechanisms presumably similar to the previously studied conjugated organic polymers,[8,9] whereas the MO properties of the radical polymers are modified by the paramagnetic moieties along the main chain. However, it will be necessary to measure a continuous Faraday rotation spectrum, across the entire vis–NIR range, to establish how universal this effect is. This unexpected discovery provides us an alternative way to tune the sign of Faraday rotation, which could be useful for specific magnetic and photonic device applications.

7. CONCLUSION

In summary, we have developed BDPA-based conjugated radical polymers and studied their redox activity, conductivity, and MO properties by *in situ* EPR spectroelectrochemistry, *in situ* conductivity measurements, and Faraday rotation measurements. The radical polymers were demonstrated to be ambipolar (capable of oxidation and reduction) and redox-active by detailed electrochemical studies and showed superior conductivities relative to their hydrogenated analogues. DFT calculations of **P-T** and **RP-T** reveal that the radical polymer possesses higher planarity than the hydrogenated form when oxidatively doped, which facilitates interchain packing and charge migration. The existence of unpaired electrons in the radical polymers affords them unique MO activities with the possibility to tune the sign of Faraday rotation, and they give absolute Verdet constants up to $(2.80 \pm 0.84) \times 10^4$ deg T^{-1} m^{-1} at 532 nm, making them a promising new type of paramagnetic MO material.

■ ASSOCIATED CONTENT

Supporting Information

The Supporting Information is available free of charge on the ACS Publications website at DOI: 10.1021/jacs.8b06193.

Experimental procedures, details of synthesis and the characterization of polymers and monomers, EPR spectroelectrochemistry, theoretical calculations, ^{1}H, ^{13}C, and ^{31}P NMR spectra (PDF)

■ AUTHOR INFORMATION

Corresponding Author

*tswager@mit.edu

ORCID

Pan Wang: 0000-0001-9137-702X
Sibo Lin: 0000-0001-5922-6694
Martin D. Peeks: 0000-0002-9057-9444
Timothy M. Swager: 0000-0002-3577-0510

Notes

The authors declare no competing financial interest.

■ ACKNOWLEDGMENTS

This work was funded by the Air Force Office of Scientific Research. S.L. was supported by NIH F32 NRSA (#GM110897). Z.L. thanks the Energy Frontier Research Center for Excitonics sponsored by U.S. Department of Energy for support of theoretical studies. M.D.P. thanks the English-Speaking Union for a Lindemann Trust Fellowship. We thank Dr. Ralph T. Weber and Dr. Thach V. Can for EPR measurements and useful discussions.

DOI: 10.1021/jacs.8b06193
J. Am. Chem. Soc. 2018, 140, 10881–10889

REFERENCES

(1) (a) Rajca, A. *Chem. Rev.* **1994**, *94*, 871−893. (b) Nishide, H. *Adv. Mater.* **1995**, *7*, 937−941.

(2) (a) Baev, A.; Prasad, P. N. *Opt. Mater. Express* **2017**, *7*, 2432−2439. (b) Baev, A.; Prasad, P. N.; Ågren, H.; Samoć, M.; Wegener, M. *Phys. Rep.* **2015**, *594*, 1−60. (c) Lvovsky, A. I.; Sanders, B. C.; Tittel, W. *Nat. Photonics* **2009**, *3*, 706−714. (d) Lenz, J.; Edelstein, S. *IEEE Sens. J.* **2006**, *6*, 631−649.

(3) (a) Muench, S.; Wild, A.; Friebe, C.; Häupler, B.; Janoschka, T.; Schubert, U. S. *Chem. Rev.* **2016**, *116*, 9438−9484. (b) Tomlinson, E. P.; Hay, M. E.; Boudouris, B. W. *Macromolecules* **2014**, *47*, 6145−6158. (c) Janoschka, T.; Hager, M. D.; Schubert, U. S. *Adv. Mater.* **2012**, *24*, 6397−6409. (d) Oyaizu, K.; Nishide, H. *Adv. Mater.* **2009**, *21*, 2339−2344.

(4) (a) Nishide, H.; Yoshioka, N.; Kaneko, T.; Tsuchida, E. *Macromolecules* **1990**, *23*, 4487−4488. (b) Nishide, H.; Yoshioka, N.; Inagaki, K.; Tsuchida, E. *Macromolecules* **1988**, *21*, 3119−3120. (c) Korshak, Y. V.; Medvedeva, T. V.; Ovchinnikov, A. A.; Spector, V. N. *Nature* **1987**, *326*, 370.

(5) (a) Buckingham, A.; Stephens, P. *Annu. Rev. Phys. Chem.* **1966**, *17*, 399−432. (b) Faraday, M. *Philos. Trans. R. Soc. London* **1846**, *136*, 1−20.

(6) (a) Stadler, B. J.; Mizumoto, T. *IEEE Photonics J.* **2014**, *6*, 1−15. (b) Tien, M.-C.; Mizumoto, T.; Pintus, P.; Kromer, H.; Bowers, J. E. *Opt. Express* **2011**, *19*, 11740−11745. (c) Śmigaj, W.; Romero-Vivas, J.; Gralak, B.; Magdenko, L.; Dagens, B.; Vanwolleghem, M. *Opt. Lett.* **2010**, *35*, 568−570. (d) Shoji, Y.; Mizumoto, T.; Yokoi, H.; Hsieh, I.-W.; Osgood, R. M., Jr *Appl. Phys. Lett.* **2008**, *92*, 071117.

(7) (a) Hafez, J.; Gao, J.; Eden, J. *Appl. Phys. Lett.* **2007**, *90*, 132502. (b) Lenz, J. E. *Proc. IEEE* **1990**, *78*, 973−989.

(8) Gangopadhyay, P.; Koeckelberghs, G.; Persoons, A. *Chem. Mater.* **2011**, *23*, 516−521.

(9) Root, S. E.; Savagatrup, S.; Printz, A. D.; Rodriquez, D.; Lipomi, D. J. *Chem. Rev.* **2017**, *117*, 6467−6499.

(10) (a) Vandendriessche, S.; Van Cleuvenbergen, S.; Willot, P.; Hennrich, G.; Srebro, M.; Valev, V. K.; Koeckelberghs, G.; Clays, K.; Autschbach, J.; Verbiest, T. *Chem. Mater.* **2013**, *25*, 1139−1143. (b) Araoka, F.; Abe, M.; Yamamoto, T.; Takezoe, H. *Appl. Phys. Express* **2009**, *2*, 011501. (c) Gangopadhyay, P.; Voorakaranam, R.; Lopez-Santiago, A.; Foerier, S.; Thomas, J.; Norwood, R. A.; Persoons, A.; Peyghambarian, N. *J. Phys. Chem. C* **2008**, *112*, 8032−8037. (d) Koeckelberghs, G.; Vangheluwe, M.; Doorsselaere, K. V.; Robijns, E.; Persoons, A.; Verbiest, T. *Macromol. Rapid Commun.* **2006**, *27*, 1920−1925.

(11) Lim, C. K.; Cho, M. J.; Singh, A.; Li, Q.; Kim, W. J.; Jee, H. S.; Fillman, K. L.; Carpenter, S. H.; Neidig, M. L.; Baev, A.; Swihart, M. T.; Prasad, P. N. *Nano Lett.* **2016**, *16*, 5451−5455.

(12) (a) Sato, K.; Ichinoi, R.; Mizukami, R.; Serikawa, T.; Sasaki, Y.; Lutkenhaus, J.; Nishide, H.; Oyaizu, K. *J. Am. Chem. Soc.* **2018**, *140*, 1049−1056. (b) Joo, Y.; Agarkar, V.; Sung, S. H.; Savoie, B. M.; Boudouris, B. W. *Science* **2018**, *359*, 1391−1395.

(13) (a) Li, F.; Gore, D. N.; Wang, S.; Lutkenhaus, J. L. *Angew. Chem., Int. Ed.* **2017**, *56*, 9856−9859. (b) Li, F.; Zhang, Y.; Kwon, S. R.; Lutkenhaus, J. L. *ACS Macro Lett.* **2016**, *5*, 337−341. (c) Goto, H.; Koyano, T.; Ikeda, H.; Yoshizaki, R.; Akagi, K. *Polymer* **2004**, *45*, 4559−4564.

(14) (a) Can, T. V.; Weber, R. T.; Walish, J. J.; Swager, T. M.; Griffin, R. G. *Angew. Chem., Int. Ed.* **2017**, *56*, 6744−6748. (b) Michaelis, V. K.; Smith, A. A.; Corzilius, B. r.; Haze, O.; Swager, T. M.; Griffin, R. G. *J. Am. Chem. Soc.* **2013**, *135*, 2935−2938.

(15) Koelsch, C. *J. Am. Chem. Soc.* **1957**, *79*, 4439−4441.

(16) Nishide, H.; Yoshioka, N.; Saitoh, Y.; Gotoh, R.; Miyakawa, T.; Tsuchida, E. *J. Macromol. Sci., Part A: Pure Appl.Chem.* **1992**, *29*, 775−786.

(17) (a) Dane, E. L.; Swager, T. M. *J. Org. Chem.* **2010**, *75*, 3533−3536. (b) Dane, E. L.; Maly, T.; Debelouchina, G. T.; Griffin, R. G.; Swager, T. M. *Org. Lett.* **2009**, *11*, 1871−1874.

(18) (a) Chaudhari, S. R.; Wisser, D.; Pinon, A. C.; Berruyer, P.; Gajan, D.; Tordo, P.; Ouari, O.; Reiter, C.; Engelke, F.; Copéret, C.; Lelli, M.; Lesage, A.; Emsley, L. *J. Am. Chem. Soc.* **2017**, *139*, 10609−10612. (b) Ni, Q. Z.; Daviso, E.; Can, T. V.; Markhasin, E.; Jawla, S. K.; Swager, T. M.; Temkin, R. J.; Herzfeld, J.; Griffin, R. G. *Acc. Chem. Res.* **2013**, *46*, 1933−1941.

(19) Kuhn, R.; Neugebauer, A. *Monatsh. Chem.* **1964**, *95*, 3−23.

(20) (a) Breslin, D. T.; Fox, M. A. *J. Phys. Chem.* **1993**, *97*, 13341−13347. (b) Dane, E. L.; Swager, T. M. *Org. Lett.* **2010**, *12*, 4324−4327.

(21) (a) Lin, F.; Pei, D.; He, W.; Huang, Z.; Huang, Y.; Guo, X. *J. Mater. Chem.* **2012**, *22*, 11801−11807. (b) Tang, Y.; He, F.; Yu, M.; Wang, S.; Li, Y.; Zhu, D. *Chem. Mater.* **2006**, *18*, 3605−3610. (c) Green, A. G., II; Singer, L. A.; Parks, J. H. *J. Chem. Phys.* **1973**, *58*, 2690−2695.

(22) Eaton, G. R.; Eaton, S. S.; Barr, D. P.; Weber, R. T. Standard Samples. In *Quantitative EPR: A Practitioners Guide*; Springer Vienna: Vienna, 2010; pp 107−113.

(23) Kittlesen, G. P.; White, H. S.; Wrighton, M. S. *J. Am. Chem. Soc.* **1984**, *106*, 7389−7396.

(24) (a) Nguyen, M. T.; Jones, R. A.; Holliday, B. J. *Macromolecules* **2017**, *50*, 872−883. (b) Rochat, S. b.; Swager, T. M. *J. Am. Chem. Soc.* **2013**, *135*, 17703−17706. (c) Swager, T. M. *Acc. Chem. Res.* **1998**, *31*, 201−207. (d) Pickup, P.; Kutner, W.; Leidner, C.; Murray, R. W. *J. Am. Chem. Soc.* **1984**, *106*, 1991−1998.

(25) Wang, P.; Jeon, I.; Lin, Z.; Peeks, M. D.; Savagatrup, S.; Kooi, S. E.; Van Voorhis, T.; Swager, T. M. *J. Am. Chem. Soc.* **2018**, *140*, 6501−6508.

DOI: 10.1021/jacs.8b06193
J. Am. Chem. Soc. 2018, 140, 10881−10889